ISSN 1063-7850, Technical Physics Letters, 2015, Vol. 41, No. 7, pp. 697–700. © Pleiades Publishing, Ltd., 2015.
Original Russian Text © V.I. Ivashchenko, A.D. Pogrebnjak, O.V. Sobol', V.N. Rogoz, A.A. Meilekhov, S.N. Dub, A.I. Kupchishin, 2015, published in Pis'ma v Zhurnal Tekhnicheskoi Fiziki, 2015, Vol. 41, No. 14, pp. 72–78.

The Effect of Al Target Current on the Structure and Properties of (Nb_2Al)N Films with an Amorphous AlN Phase

V. I. Ivashchenko[a], A. D. Pogrebnjak[b]*, O. V. Sobol'[c], V. N. Rogoz[b], A. A. Meilekhov[c], S. N. Dub[d], and A. I. Kupchishin[e]

[a] *Institute for Problems in Materials Science, National Academy of Sciences of Ukraine, 03680 Kyiv-142, Ukraine*
[b] *Sumy National University, 40007 Sumy, Ukraine*
[c] *National Technical University Kharkiv Polytechnic Institute, 61002 Kharkiv, Ukraine*
[d] *V. Bakul Institute for Superhard Materials, 04074 Kyiv, Ukraine*
[e] *Abai Kazakh National Pedagogical University, Almaty, 050010 Kazakhstan*
**e-mail: alexp@i.ua*

Received January 20, 2015

Abstract—Nanocomposite films based on (Nb_2Al)N intermetallic nitride have been obtained by the method of magnetron sputtering. X-ray diffraction analysis revealed two stable states of the crystalline structure: (i) NbN with low amount (within 5 at %) of dissolved Al in a composition close to (Nb_2Al)N and (ii) an amorphous component related to aluminum nitride formed by reactive magnetron sputtering. The substructural characteristics (grain size and microdeformation level) are sensitive to the current via Al target and exhibit correlation with nanohardness and Knoop hardness of the film, which vary within 29–33.5 and 46–48 GPa, respectively.

DOI: 10.1134/S1063785015070214

Films and coatings based on niobium nitride (NbN) exhibit many interesting properties, such as high hardness, electric conductivity, thermal stability, and chemical inertness [1]. NbN films are used as cathode material for field electron emission devices in vacuum microelectronics [2]. It was established that the introduction of Al atoms into the crystalline lattice of NbN leads to the formation of $Nb_{1-x}Al_xN$ solid solutions.

Arc-deposited $Nb_{1-x}Al_xN$ coatings with $x < 0.45$ are formed predominantly with the cubic B1 (NaCl type) structure; for $x = 0.45$–0.71, a mixture of B1 and B4 structures has been observed, while $x > 0.71$ favors the formation of B4 (wurtzite type) structure [3]. Magnetron-sputter-deposited Nb–Al–N films also exhibited B1 (sometimes, with B_K–δ-NbN phase) or B4 structure, or their mixtures [4–7]. However, nanocomposite NbN/AlN films have not been studied until now. In order to fill this gap, the present study was aimed at depositing Nb–Al–N films under assumption that nanocomposite films would exhibit improved mechanical properties in comparison to $Nb_{1-x}Al_xN$ films.

Nb–Al–N films were deposited onto mirror-polished Si (100) substrates by DC magnetron sputtering of Nb (99.9%) and Al (99.999%) targets with 72 mm diameter and 4 mm thickness in argon and nitrogen atmosphere under the following conditions: substrate temperature $T_s = 350$°C, substrate bias voltage $U_B = -50$ V, gas flow rates $F_{Ar} = 40$ sccm and $F_{N2} = 13$ sccm, and working pressure $P_C = 0.17$ Pa. The current via Al target was varied within $I_{Al} = 50$, 100, 150, 200, 250, and 300 mA, which corresponded to a discharge power density of $P_{Al} = 2.9$, 5.7, 8.6, 11.4, 13.7, and 17.1 W/cm^2, respectively. The current via Nb target was $I_{Nb} = 300$ mA, which corresponded to $P_{Nb} = 17.1$ W/cm^2. The residual base pressure in the vacuum chamber was below 10^{-4} Pa. The distance from targets to the substrate holder was 8 cm, and the dihedral angle between targets was ~45°. Prior to being placed into the vacuum chamber, the substrates were ultrasonically cleaned of surface contaminations. Prior to coating deposition, the substrates were ion-etched in hydrogen plasma for 5 min.

The structure of deposited films was studied by X-ray diffraction (XRD) on a DRON-3M diffractometer using CuK_α radiation. Deconvolution of complex XRD profiles into components was performed using an original program. Substructural characteristics (grain size and microdeformation) were determined by the line shape analysis with approximation using the Cauchy function.

The Fourier transform infrared (FTIR) spectra of coatings were measured at room temperature in a 400–4000 cm^{-1} range on a TSM 1202 (Infraspek Ltd.) spectrometer. The Knoop hardness (*HK*) was measured using a Micromet 2103 (Buehler Ltd.) microhardness tester at a 100-mN load. The film thickness

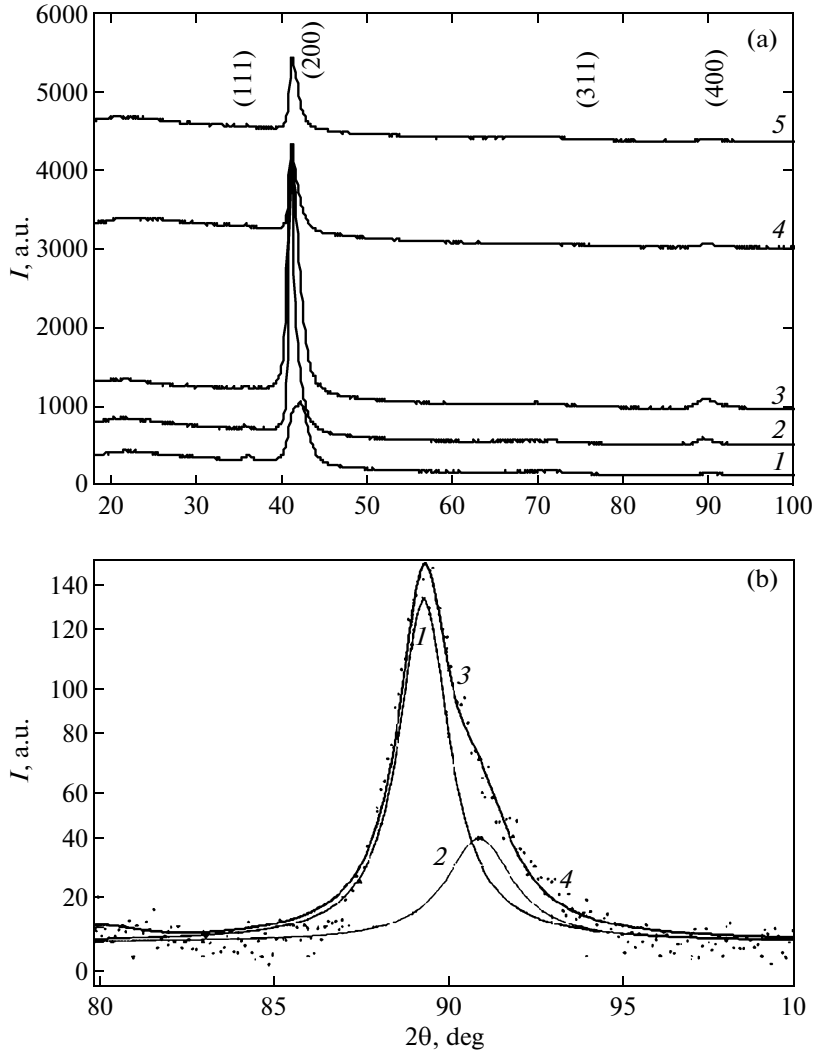

Fig. 1. (a) XRD patterns of Nb–Al–N coatings deposited at various I_{Al} (mA): (*1*) 50, (*2*) 100, (*3*) 150, (*4*) 250, and (*5*) 300; (b) deconvolution of the XRD profile of the coating deposited at I_{Al} = 150 mA into components: (*1*) NbN (400) reflection, (*2*) $Nb_{0.67}Al_{0.33}N$ (400) reflection, (*3*) sum of components, and (*4*) points of the initial data array.

was determined with the aid of a Micron-Gamma profilometer. The thicknesses of Nb–Al–N coatings ranged within $d = 0.7–0.9$ μm and were weakly dependent on I_{Al} in the interval studied.

Figure 1a shows the XRD patters of Nb–Al–N coatings deposited at various I_{Al}, where the indicated reflections refer to the B1 structure of NbN [8]. In addition, the interval of diffraction angles $2\theta = 28°–30°$ revealed a halolike diffraction component due to an amorphous phase. Based on the results of previous investigations, this component can be identified with the amorphous aluminum nitride. As can be seen, the sputtering at all I_{Al} values and a relatively small constant substrate bias voltage of –50 V leads to the formation of grains with predominant growth direction [100] perpendicular to the surface, which results in a relative increase in the (200) reflection intensity for all samples (see Fig. 1a). At a minimum value of I_{Al} = 50 mA (Fig. 1a, curve *1*), the XRD pattern exhibits a complicated profile corresponding to various planes, while higher currents lead to the appearance of asymmetry of diffraction lines on the side of greater angles. The results of deconvolution showed the presence of two characteristic periods (Fig. 1b). The first is close to 0.438–0.439 nm, which is characteristic of NbN lattice with a small amount of substitutional Al impurity. The second period is about 0.428–0.429 nm, which is characteristic of Nb–Al–N system with a Nb : Al = 2 : 1 atomic ratio in the lattice that corresponds to $Nb_{0.67}Al_{0.33}N$ formula as determined using the Vegard rule for different radii of substituted atoms in crystal lattices of the same type [9]. The base lattice parameters for B1–NbN and B1–AlN were selected to be 0.4393 and 0.4120 nm, respectively [5].

For the intermediate interval of currents, I_{Al} = 150–250 mA, the phase ratio is close to

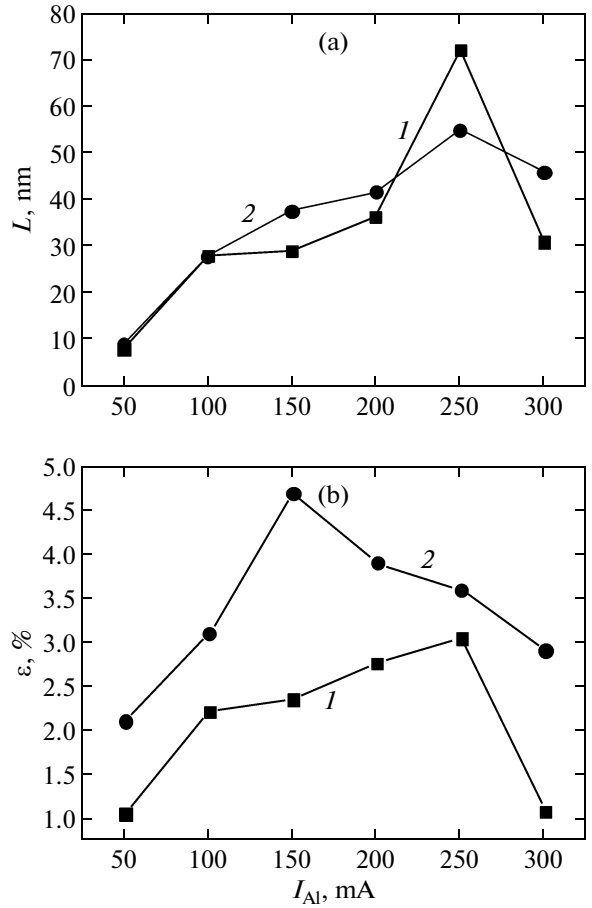

Fig. 2. Dependences of the substructural characteristics—(a) average grain size L and (b) microdeformation level ε—on Al-target current I_{Al} for the crystalline components of (*1*) NbN and (*2*) $Nb_{0.67}Al_{0.33}N$ (or $(Nb_2Al)N$).

3.5 $NbN/Nb_{0.67}Al_{0.33}N$. The corresponding substructural characteristics, which have been determined by the approximation of two orders of diffraction reflections for the (200)–(400) pair, are presented in Fig. 2. As can be seen, an increase in I_{Al} is accompanied by growth of the grain size and microdeformation level in the direction of [100] texture axis. The growth in deformation is probably explained by increasing dissolution of aluminum atoms in niobium sublattice, which leads to a strong distortion of the lattice. A sharp decrease in the grain size and microdeformation level at the maximum Al target current (I_{Al} = 300 mA) may be related to both the annealing and the ordering of defect structure with the formation of new boundaries via a grain-polygonization-type process.

We have also deposited AlN coatings at various I_{Al} values and analyzed the corresponding XRD patterns. The results (not presented here) showed that all AlN films were amorphous (a-AlN). However, their FTIR spectra were indicative of the improvement of Al–N bonds with increasing I_{Al} (a line at 667 cm^{-1} related to Al–N bond vibrations [10, 11] became more pronounced).

Figure 3 shows the results of nano- and microindentation of the obtained $(Nb_2Al)N$ nanocomposite films. The Knoop hardness (*HK*) of Nb–Al–N films was higher than that of NbN and AlN films. The mechanical strength of nanocomposite films was also better than that of $Nb_{1-x}Al_xN$ films. It was noted that the Knoop microhardness is about 50% greater than the nanohardness, which may be related to the fact that nanoindentation proceeds in a dynamic regime, while the Knoop hardness is measured in a static regime.

Thus, we have found two stable crystalline states in nanocomposite films: (i) NbN with low amount (within 5 at %) of dissolved Al in a composition close to $(Nb_2Al)N$ and (ii) an amorphous component related to aluminum nitride formed by reactive magnetron sputtering. The substructural characteristics are sensitive to the current via the Al target and exhibit correlation with the nanohardness and Knoop hardness of the film. The good mechanical properties of the obtained nanocomposite films allow them to be

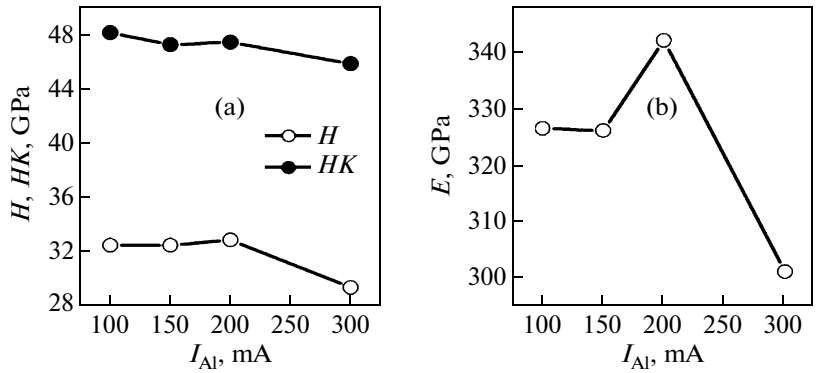

Fig. 3. Plots of (a) nanohardness (*H*) and Knoop hardness (*HK*) and (b) elastic modulus (*E*) vs. Al-target current I_{Al} for magnetron-sputter-deposited Nb–Al–N films.

recommended as wear-resistant and protective coatings.

Acknowledgments. This study was supported in part in the framework of a State Complex Research Program, projects nor. 0112U001382 and 0113U000137c.

REFERENCES

1. S. A. Barnett, A. Madan, I. Kim, and K. Martin, MRS Bull. **28**, 169 (2003).
2. Y. Gotoh, M. Nagao, T. Ura, H. Tsuji, and J. Ishikawa, Nucl. Instrum. Methods. Phys. Res., Sect. B **148** (1–4), 925 (1999).
3. R. Franz, M. Lechthaler, C. Polzer, and C. Mitterer, Surf. Coat. Technol. **204**, 2447 (2010).
4. Y. Makino, K. Saito, Y. Murakami, and K. Asami, Solid State Phenom. **127**, 195 (2007).
5. H. C. Barshilla, B. Deepthi, and K. S. Rajam, J. Mater. Res. **23**, 1258 (2008).
6. T. I. Selinder, D. J. Miller, and K. E. Gray, Vacuum **46** (12), 1401 (1995).
7. D. Holec, R. Franz, P. H. Mayrhofer, and C. Mitterer, J. Phys. D: Appl. Phys. **41**, 145403 (2010).
8. ICDD X-ray powder diffraction file [038-1155].
9. Ya. S. Umanskii and Yu. A. Skakov, *Metal Physics: Atomic Structure of Metals and Alloys* (Atomizdat, Moscow, 1978) [in Russian].
10. K. Jadannadham, A. K. Sharma, Q. Wei, R. Kalyanraman, and J. Narayan, J. Vac. Sci. Technol. A **16**, 2804 (1998).
11. A. D. Pogrebnjak, G. Abadias, O. V. Bondar, O. V. Sobol, V. M. Beresnev, A. V. Pshyk, A. A. Demianenko, K. O. Belovol, D. A. Kolesnikov, and H. Komsta, Acta Phys. Pol. A **125**, 1284 (2014).

Translated by P. Pozdeev